

Northumbria Research Link

Citation: Maramizonouz, Sadaf, Jia, Changfeng, Rahmati, Mohammad, Liu, Qiang, Torun, Hamdi, Wu, Qiang and Fu, Yong Qing (2022) Acoustofluidic Patterning inside Capillary Tubes Using Standing Surface Acoustic Waves. *International Journal of Mechanical Sciences*, 214. p. 106893. ISSN 0020-7403

Published by: Elsevier

URL: <https://doi.org/10.1016/j.ijmecsci.2021.106893>
<<https://doi.org/10.1016/j.ijmecsci.2021.106893>>

This version was downloaded from Northumbria Research Link:
<http://nrl.northumbria.ac.uk/id/eprint/47555/>

Northumbria University has developed Northumbria Research Link (NRL) to enable users to access the University's research output. Copyright © and moral rights for items on NRL are retained by the individual author(s) and/or other copyright owners. Single copies of full items can be reproduced, displayed or performed, and given to third parties in any format or medium for personal research or study, educational, or not-for-profit purposes without prior permission or charge, provided the authors, title and full bibliographic details are given, as well as a hyperlink and/or URL to the original metadata page. The content must not be changed in any way. Full items must not be sold commercially in any format or medium without formal permission of the copyright holder. The full policy is available online: <http://nrl.northumbria.ac.uk/policies.html>

This document may differ from the final, published version of the research and has been made available online in accordance with publisher policies. To read and/or cite from the published version of the research, please visit the publisher's website (a subscription may be required.)



Contents lists available at ScienceDirect

International Journal of Mechanical Sciences

journal homepage: www.elsevier.com/locate/ijmecsci

Acoustofluidic Patterning inside Capillary Tubes Using Standing Surface Acoustic Waves

Sadaf Maramizonouz^a, Changfeng Jia^b, Mohammad Rahmati^{a,*}, Tengfei Zheng^b, Qiang Liu^c, Hamdi Torun^a, Qiang Wu^a, Yongqing Fu^a^a Faculty of Engineering & Environment, Northumbria University, Newcastle upon Tyne, NE1 8ST, UK^b State Key Laboratory for Manufacturing Systems Engineering, Xian Jiaotong University, 710049, Xian, 710048, P.R. China^c State Key Laboratory of Synthetical Automation for Process Industries, School of Control Engineering, North-eastern University at Qinhuangdao, 066004, P.R. China

ARTICLE INFO

Keywords:

Acoustic Manipulation
Capillary Tubes
Particle Patterning
Acoustofluidics
Numerical Simulation
Thin Film SAW Devices

ABSTRACT

Acoustofluidic platforms have great potentials to integrate capillary tubes for controlling and manipulating microparticles and biological cells in both non-flowing and continuous-flow settings. In order to effectively manipulate microparticles/cells inside capillary tubes, it is essential to fully understand and control the patterns generated inside the capillary tubes with different cross-sections, and to investigate the influences of configuration and position arrangement of electrodes along with the capillary tubes. This paper aims to systematically investigate the patterning and alignment of microparticles inside glass capillary tubes using thin film surface acoustic wave (SAW) devices. Through both experimental studies and numerical modelling, effects of various cross-section geometries of the capillary tubes and their positioning with respect to the direction of interdigital transducers (IDTs) of the SAW device in both a stationary fluid and a continuous flow fluid were studied. Results showed that for the rectangular glass capillary tubes, the patterned lines of particles are parallel to the tube's side walls, irrelevant to the tube positions along with the IDTs, which is mainly caused by the standing wave field generated inside the rectangular glass tube. Whereas for the circular glass capillary tubes, alignment patterns of particles are quite different along the tube's height. At the bottom of the circular tube, particles are patterned into lines parallel to the tube direction, because the acoustic waves propagate into the water and form a standing wave along the direction of the circular tube. Whereas at the middle height of the tube, the particles are patterned into lines perpendicular to the tube direction, because the formed standing waves also propagate around the circular cross-section of the tube and are perpendicular to the tube direction. For the cases with a continuous liquid flow, under the agitation of acoustic waves, particles are patterned in lines parallel to the flow directions for both the rectangular and circular glass tubes, and the fluid flow enhances and smoothens the patterned lines of the particles.

1. Introduction

Conventional acoustofluidic platforms are usually comprised of microfluidic elements (such as microchannel) and acoustic elements (such as ultrasonic or acoustic wave devices) [1,2]. These platforms have been utilized for contact-free manipulation, patterning, sorting [3–5] and separation [6–9] of microparticles and biological cells, in various chemical and biomedical applications including cell studies

[10], cancer diagnosis and tissue engineering [1,11–14]. Microfluidic elements, i.e., microchambers and microchannels, are usually fabricated in a clean-room environment using materials such as polydimethylsiloxane (PDMS) [3–5, 8,9], silicone elastomer [15], polymethyl methacrylate (PMMA) [16,17], or glass [7,18,19]. Alternatively, capillary tubes have also been integrated with acoustic devices and used to trap [20–28], focus [29–35], align and pattern [36–40], separate [41, 42], deform [43], enrich [44,45], arrange [46], and manipulate [47] microparticles and biological cells [48]. For example, Lata et al. [36]

Abbreviations: ARF, acoustic radiation force; DC, direct current; DI, deionised; FEM, finite element method; IDT, interdigital transducer; LiNbO₃, lithium niobate; PDMS, polydimethylsiloxane; PMMA, polymethyl methacrylate; RF, radio frequency; SAW, surface acoustic wave; SSAW, standing surface acoustic wave; ZnO, zinc oxide.

* Corresponding authors:-Dr. Mohammad Rahmati

E-mail addresses: mohammad.rahmati@northumbria.ac.uk (M. Rahmati), richard.fu@northumbria.ac.uk (Y. Fu).<https://doi.org/10.1016/j.ijmecsci.2021.106893>

Received 9 June 2021; Received in revised form 12 October 2021; Accepted 24 October 2021

Available online 27 October 2021

0020-7403/© 2021 The Author(s). Published by Elsevier Ltd. This is an open access article under the CC BY license (<http://creativecommons.org/licenses/by/4.0/>).

Nomenclature*Latin Symbols*

A_x	m wave's displacement amplitude in the x direction
A_y	m wave's displacement amplitude in the y direction
Cd	- wave attenuation coefficient
c_f	m/s wave speed in the fluid
D	N viscous drag force
d	m particle diameter
E	N/m ² Young's modulus
F_{AR}	N acoustic radiation force
F_{ARx}	N acoustic radiation force in the x direction
F_s	N/m ³ load per unit volume
k	- wavenumber
P_{ac}	Pa acoustic pressure amplitude
P_{in}	Pa acoustic pressure field of the incoming wave
R	m position vector
r	m particle radius
U_f	m/s fluid velocity vector
U_p	m/s particle velocity vector
U_s	m solid displacement vector
$u_x - wall$	m/s SAW velocity in the x direction
$u_y - wall$	m/s SAW velocity in the y direction
V_{in}	m/s velocity field of the incoming wave
W	m width of the fluid channel
x	m particle distance from the nearest pressure node

Greek Symbols

β	rad angle between the capillary tubes and the IDTs
β_f	m ² /N fluid compressibility

β_p	m ² /N particle compressibility
δ	m thickness of the viscous, acoustic boundary layer
ε	- strain tensor
ζ	- ratio of the displacement amplitudes
λ	m wavelength
μ_f	Pa.s fluid viscosity
ρ_f	kg/m ³ fluid density
ρ_p	kg/m ³ particle density
σ	Pa stress tensor
τ_p	s particle characteristic time
\varnothing_s	- acoustic contrast factor
ω	Hz wave's angular frequency

Other Symbols

\forall_p	m ³ particle volume
-------------	--------------------------------

Abbreviations

ARF	acoustic radiation force
DC	direct current
DI	deionised
FEM	finite element method
IDT	interdigital transducer
LiNbO ₃	lithium niobate
PDMS	polydimethylsiloxane
PMMA	polymethyl methacrylate
RF	radio frequency
SAW	surface acoustic wave
SSAW	standing surface acoustic wave
ZnO	zinc oxide

and Lisa et al. [46] used capillary tubes to immobilise biological cells in a cured gel to form a fibre with fixed positions of the cells. Mishra et al. [43] performed deformation of red blood cells using acoustic radiation forces inside a capillary tube.

For continuous-flow applications, Raiton et al. [20], Gralinski et al. [21], O'Mahoney et al. [22], and Hammarström et al. [23–25] used capillary tubes with circular [20,21], square [22], and rectangular [23–25] cross-sections to trap microparticles within a flowing liquid, with the direction of the acoustic radiation force opposite to the liquid flow direction. Glynne-Jones et al. [26] utilised a one-dimensional piezoelectric array to trap microparticles at the centreline of a capillary tube with a rectangular cross-section and then transported them along the length of the tube. Fornell et al. [27] successfully trapped hydrogel droplets inside a rectangular capillary tube using acoustic forces. Fornell et al. [28] demonstrated “binary trapping” of microparticles based on their densities in a high-density fluid inside a capillary tube with a rectangular cross-section. Early studies of acoustic focusing of microparticles inside capillary tubes with circular and square cross-sections have been done by Goddard et al. [29] and Perfetti et al. [30], respectively. Li et al. [32], and Lei et al. [34,35] used two piezoelectric transducers to perform two-dimensional microparticle focusing inside square and circular capillary tubes. For biological applications, Galanzha et al. [31] and Gonzalez et al. [33] used acoustic waves to focus and enrich blood cells inside capillary tubes with circular and square cross-sections. Additionally, Piyasena et al. [40] developed an acoustofluidic device for patterning and alignment of microparticles using rectangular capillary tubes. They were successful in aligning microparticles with different sizes into parallel lines inside the capillary tube.

The capillary tubes, are generally disposable, low-cost, optically transparent, and easy to use within the acoustofluidic setups. They also offer high acoustic quality and do not require additional bonding of

various acoustofluidic components [48]. They are normally made of glass [21–36, 38–41, 43–47], but sometimes polyimide [37] and cellulose [20]. Capillary tubes have various cross-section shapes, such as circular [20,21,29,31,34–36, 41,46,47], square [22,30,32,33,37,39,41,43] and rectangular [23–28, 38,40], which makes them good candidates for various acoustofluidic applications [48].

To understand the mechanisms and principles of particle manipulation inside capillary tubes, there have been a few studies on modelling of the acoustofluidics platforms integrated with capillary tubes [22,23,38, 43,44,47]. For example, Gralinski et al. simulated effects of different configurations of piezoelectric transducers connected to a circular glass capillary for particle trapping [21,49]. Ley and Bruss performed three dimensional numerical modelling of particles trapped inside a glass capillary tube with a rectangular cross-section [50]. Bach and Bruus further proposed a theory for particle trapping inside glass capillary tubes with arbitrary cross-sections [51]. Additionally, the convective flow and heat transfer [52], natural [53] and mixed [54] convections, and hydrodynamic stability of heat transfer [55] inside vertically positioned circular capillaries induced by various heat sources have been theoretically analysed and numerically modelled.

Capillary tubes are the potential substitutes for the conventional microchannels and can be easily integrated with surface acoustic wave (SAW) devices either without a liquid flow (for example, in a closed chamber) or in a continuous-flow condition for manipulating microparticles and cells. They can also be used to produce particles or cell fibres embedded inside a cured gel. However, various patterns generated using different cross-sections of capillary tubes, or positioning the capillary tubes along different directions compared with the SAW electrodes, have not been systematically studied. Moreover, previous studies have been focused on rigid SAW devices based on the brittle lithium niobate (LiNbO₃) for enriching [44], aligning [36], and patterning [37] microparticles and cells. Whereas so far there are no reports on using

flexible thin film SAW devices, which have advantages such as easy integration with microelectronics and other technologies, high power and high speed capabilities [56], and potential applications in flexible microfluidic platforms, body conforming wearable devices, and soft robotics [57–60].

In this paper, we systematically studied the patterning and alignment of microparticles inside glass capillary tubes using a zinc oxide (ZnO) thin-film-based flexible SAW device and capillary tubes with circular or rectangular cross-sections and at different tube positioning angles relative to the direction of the IDTs, as illustrated in Fig. 1. We performed experiments to study the particle patterning inside capillary tubes with different cross-sections using three different sizes of rectangular (Fig. 1 (a-1)) and circular (Fig. 1(b-1)) capillary tubes. We also investigated the effects of positioning the tubes on the SAW device at different angles in relation to the IDT directions (β). Additionally, we used both the rectangular and circular capillary tubes in a continuous-flow setup (Fig. 1(a-2) and (b-2)) and studied the effects of flow rates on the particle patterning and alignment inside the tube. We also developed computational models of the acoustofluidic platform and capillary tubes to explain the observed particle patterns.

2. Experimental Details

To visualise particle patterning under the effect of SAWs, glass capillary tubes with a length of ~ 2 cm and various cross-sections of rectangular (with three sizes of $4.5 \text{ mm} \times 1.0 \text{ mm}$, $3.5 \text{ mm} \times 0.8 \text{ mm}$, and $2.3 \text{ mm} \times 0.5 \text{ mm}$ which was mainly used for continuous-flow experiments) and circular (with diameter of 1.0 mm) were placed on the SAW device's surface. Deionised (DI) water droplet of $\sim 1.0 \mu\text{L}$ was added under the glass tube to effectively transfer the wave energy from the SAW device into the glass tube. The glass capillary tube was then filled with a suspension of DI water with silica microparticles (with a diameter of $5 \mu\text{m}$ and a density of 1900 kg/m^3). To further study the

formed patterns in a continuous flow of DI water in the tube, the fluid/particle mixture was pumped into the glass capillary tubes using a syringe pump (ExiGo pump) at the inlet and the mixtures was collected into a vial at the outlet. A continuous flow rate of $0.2 \mu\text{L/s}$ was applied.

The SAW devices were fabricated by depositing ZnO film (with a thickness of $\sim 5 \mu\text{m}$) onto an aluminium foil substrate (thickness of $50 \mu\text{m}$) using a direct current (DC) magnetron sputter (NS3750, Nordiko) [12,61]. The interdigital transducers (IDTs, made from $20/100 \text{ nm}$ thick of Cr/Au) of the SAW devices were fabricated using a standard photolithography and lift-off process. The designed IDTs had a wavelength of $160 \mu\text{m}$ and a frequency of 13.12 MHz . A radio frequency (RF) function generator (AIM-TTI Instruments TG5011A) was connected to an amplifier (Amplifier Research 75A) to generate the RF signals to drive the IDTs of the SAW device at its resonant frequency. A video camera (iDS, UI-3880CP-C-HQ-R2) was used to capture the motions of the fluid and the microparticles. The open-source image processing software "ImageJ" was used to post-process the recorded images and to measure the line distances.

3. Theoretical Analysis and Simulation Details

3.1. Theoretical Analysis

When two SAWs with the same frequency and amplitude travelling in the opposite directions meet each other, their constructive or destructive interferences superpose, thus generating standing SAWs (SSAWs). As the SAWs come into contact with the fluid, the acoustic energy is dissipated into the fluid and an acoustic field is generated inside the liquid. The particles suspended in the fluid are then subjected to acoustic radiation forces [62]. The acoustic radiation force (ARF) was first calculated analytically by King [63]. He presented the ARF on rigid spheres suspended in an ideal liquid (no viscosity) using perturbation methods. The calculations were broadened to include the spheres'

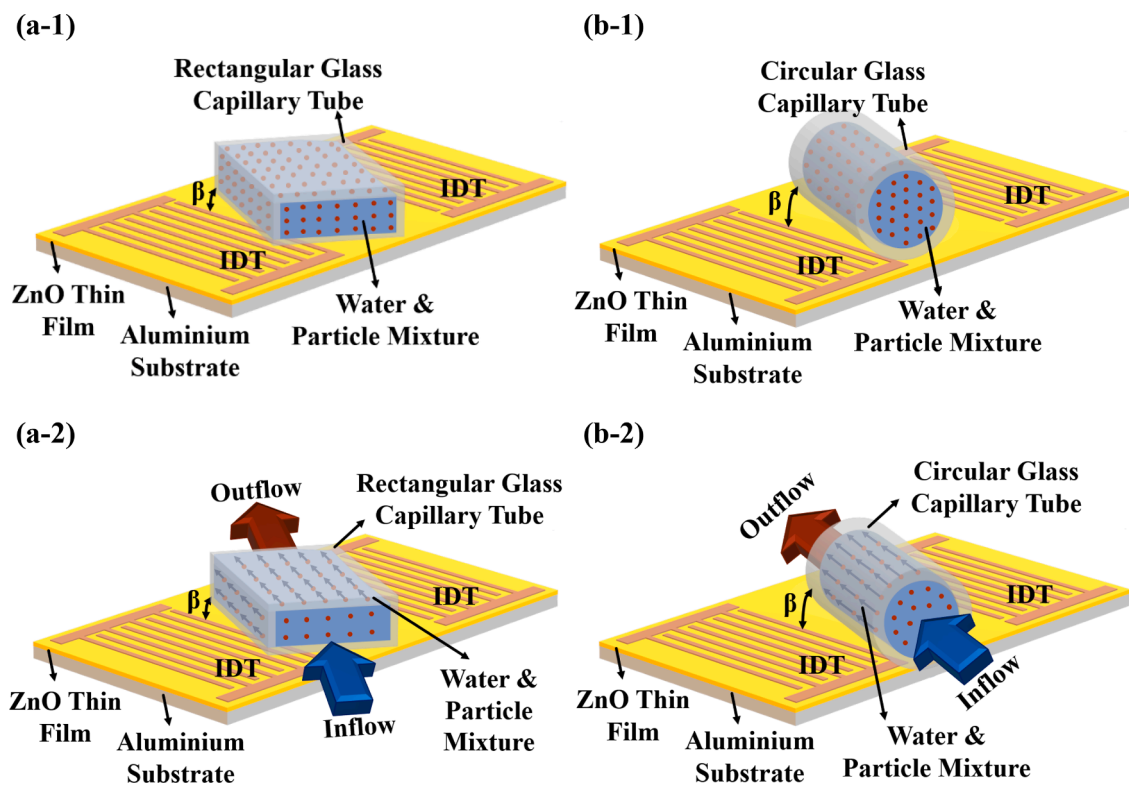


Fig. 1. Schematic illustrations of particle patterning inside glass capillary tube with (a) rectangular and (b) circular cross-section with an incline angle regarding the direction of IDTs; (1) without flow and (2) with continuous flow in the capillary tubes. To transfer the wave energy from the SAW device into the glass tube, a water droplet of $\sim 1.0 \mu\text{L}$ was added under the tube.

compressibility by Yosioka and Kawasima [64]. Gorkov [65] summarised and generalised the analytical investigations of the ARFs and Doi-nikov extended the ARF calculations to account for the effects of fluids viscosity for rigid [66] and compressible [67] spheres.

For a spherical particle dispersed in a fluid in a standing acoustic wave field, the acoustic radiation force, F_{AR} , is described as follows [63–68]:

$$F_{AR} = \frac{-4\pi}{3}r^3 \left[f_1(\tilde{\beta})\beta_f(P_{in}\nabla P_{in}) - f_2(\tilde{\rho})\rho_f \frac{3}{2} \langle (V_{in} \cdot \nabla) V_{in} \rangle \right] \quad (1)$$

$$f_1(\tilde{\beta}) = 1 - \tilde{\beta} \text{ with } \tilde{\beta} = \frac{\beta_p}{\beta_f} \quad (2)$$

$$f_2(\tilde{\rho}) = Re \left[\frac{2[1 - \gamma(\tilde{\rho})](\tilde{\rho} - 1)}{2\tilde{\rho} + 1 - 3\gamma(\tilde{\rho})} \right] \text{ with } \tilde{\rho} = \frac{\rho_p}{\rho_f} \quad (3)$$

$$\gamma(\tilde{\rho}) = -\frac{3}{2}Re[1 + i(1 + \tilde{\rho})\tilde{\delta}] \text{ with } \tilde{\delta} = \frac{\delta}{r} \quad (4)$$

where r is the particle radius, β_f is the fluid compressibility, P_{in} is the acoustic pressure field, ρ_f is the fluid density, V_{in} is velocity field of the incoming wave, β_p is the particle compressibility, ρ_p is the particle density, $\delta = \sqrt{2(\mu_f/\rho_f)/\omega}$ is the thickness of the viscous acoustic boundary layer, and ω is the angular frequency of the acoustic wave [63–68].

In this study, silica microparticles with a compressibility of $\beta_p \approx 3 \times 10^{-11} \text{ m}^2/\text{N}$ inside water with a compressibility of $\beta_f \approx 5 \times 10^{-10} \text{ m}^2/\text{N}$ were used. Comparing the values for β_p and β_f , it can be seen that the particle's compressibility is one order of magnitude smaller than that of the fluid, and thus the effects of particle's compressibility can be neglected. In addition, in this study, water (at room temperature) was used as the working fluid and the δ value was estimated to be $0.15 \mu\text{m}$ for the SAW frequency of 13.12 MHz. Therefore, for the silica particles used in this study (with a radius of $2.5 \mu\text{m}$), the effects of viscosity was neglected [68].

Because the SSAW propagates in a plane perpendicular to the IDTs, it can be assumed as one-dimensional, and the effects of particle's compressibility and fluid viscosity on the acoustic field can be assumed to be negligible. Therefore, the ARF can be calculated using the following equations [18,63-70]:

$$F_{ARx} = \left(\frac{\pi P_{ac}^2 \forall_p \beta_f}{2\lambda} \right) \varnothing_s \sin(2kx) \quad (5)$$

$$\varnothing_s = \frac{5\rho_p - 2\rho_f}{2\rho_p + \rho_f} \quad (6)$$

where P_{ac} is the amplitude of acoustic pressure, \forall_p is the particle volume, λ is the wavelength, $k = 2\pi/\lambda$ is the wavenumber, and x is the particle distance from the nearest pressure node (or anti-node) along the wave propagation direction [18,63-70].

The acoustic radiation force resulted from the SSAW directs each particle towards either the pressure node (i.e., the minimum pressure amplitude) or the pressure antinode (i.e., the maximum pressure amplitude), depending on the mechanical and physical properties of the fluid and the particles suspended in it [7]. The symbol of \varnothing_s is called the acoustic contrast factor and its sign defines whether each particle moves towards the pressure node ($\varnothing_s > 0$) or the pressure antinode ($\varnothing_s < 0$) under the effect of acoustic radiation force [18,63-70]. Silica microparticles suspended in water ($\varnothing_s > 0$) were used in this study, which were driven to the pressure nodes.

Equation (5) shows that the radiation force due to the SSAWs has a sinusoidal distribution and its period is half of the SAW wavelength. This results in the defined distance between two adjacent pressure nodes (or anti-nodes) where the particles pattern distance is theoretically equal to

half of the wavelength [69].

Particles moving in the fluid medium also experience a viscous drag force, $D = \rho_p \frac{U_f - U_p}{\tau_p}$, which depends on the properties of the fluid and the particles as well as the relative velocity. U_f is the fluid velocity vector, U_p is the particle velocity vector, $\tau_p = \rho_p d^2/18\mu_f$ is the particle's characteristic time (the time for the particle to respond to a velocity change), d is the particle's diameter, and μ_f is the fluid viscosity [71,72].

3.2. Simulation Details

Acoustofluidic systems are multi-physics and complicated with different time and length scales. These systems operate in a wide range of length and time scales from the extra small-scale and fluctuating pressure and velocity fields of the SAWs to the large-scale pressure and velocity fields of the bulk fluid. Numerical simulation requires an accurate model of the acoustofluidic platform which can effectively represent the largely different time and length scales of the acoustic field and fluid-particle dynamic in order to provide reliable results.

The first step for numerical modelling of our acoustofluidic setup is to define the geometry of the system and generate the computational meshes. For this purpose, three-dimensional models of the glass capillary tubes filled with water and placed on the SAW device were considered. The discretization of the computational domain was done using $\sim 250,000$ and $\sim 150,000$ unstructured tetrahedral elements for the rectangular and circular tubes, respectively. The modelled geometries and meshes are shown in Fig. 2.

In order to optimise the computational grids, which could present a suitable accuracy for the computational solution while also offer a reasonable computational time, mesh dependency analysis was performed for both the capillary tube geometries. Fig. 3(a) and (b) present the results of the mesh dependency analysis for the rectangular and circular tubes, respectively. It can be seen that increasing the size of the computational grid increases the accuracy of the computational solution whereas the computational time is exponentially increased.

In order to study the acoustic fields inside the capillary tubes with circular or rectangular cross-sections placed with different directions between the capillary tube and IDTs of the ZnO SAW device, the acoustofluidics platforms were modelled. The generation and propagation of the SSAWs on the surface of the SAW device were modelled using the velocity components of the SSAWs with the oscillating wall boundary conditions. The wave velocity components are defined as follows [51]:

$$u_{x-wall} = A_y \zeta \omega \left[e^{-Cd(0.5W-x)} e^{i[-k(0.5W-x)]} + e^{-Cd(0.5W+x)} e^{i[k(0.5W-x)]} \right] \quad (7)$$

$$u_{y-wall} = A_y \omega \left[e^{-Cd(0.5W-x)} e^{i[-k(0.5W-x)-\pi/2]} - e^{-Cd(0.5W+x)} e^{i[k(0.5W-x)-\pi/2]} \right] \quad (8)$$

where u_{x-wall} and u_{y-wall} are the SAW velocity components in the x and y directions, respectively, A_y is the wave's displacement amplitude, Cd is the wave attenuation coefficient, W is the width of the fluid channel, x is the longitudinal direction, and $\zeta = A_x/A_y$ is the ratio of the displacement amplitudes in x and y directions [73].

The acoustic fields which were generated inside the fluid for both the $\sim 1.0 \mu\text{L}$ droplet added under the glass tube (to transfer the wave energy) and the water filled inside the capillary tubes were modelled using the Helmholtz equations given below [74]:

$$\nabla^2 P_{in}(R) + \frac{\omega^2}{c_f^2} P_{in}(R) = 0 \quad (9)$$

where R is position vector, and c_f is the wave speed in the fluid [74].

The behaviour and structural dynamics of both the circular and rectangular capillary tubes under the effects of the SSAWs were modelled using the Hooke's Law given below [74]:

$$\sigma = E\varepsilon \quad (10)$$

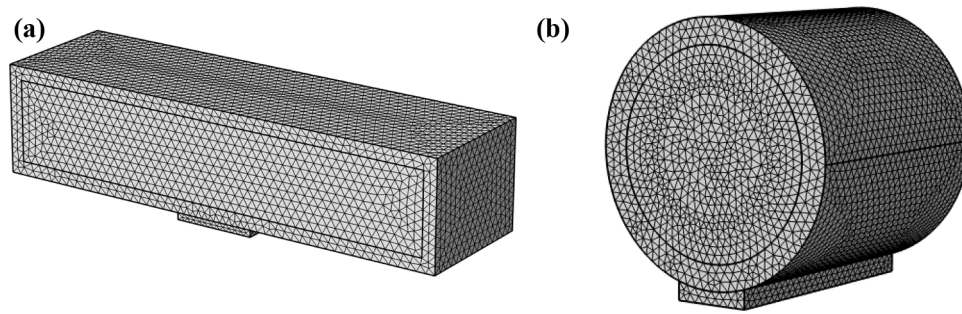


Fig. 2. Geometry and computational mesh for (a) rectangular, and (b) circular microtubes.

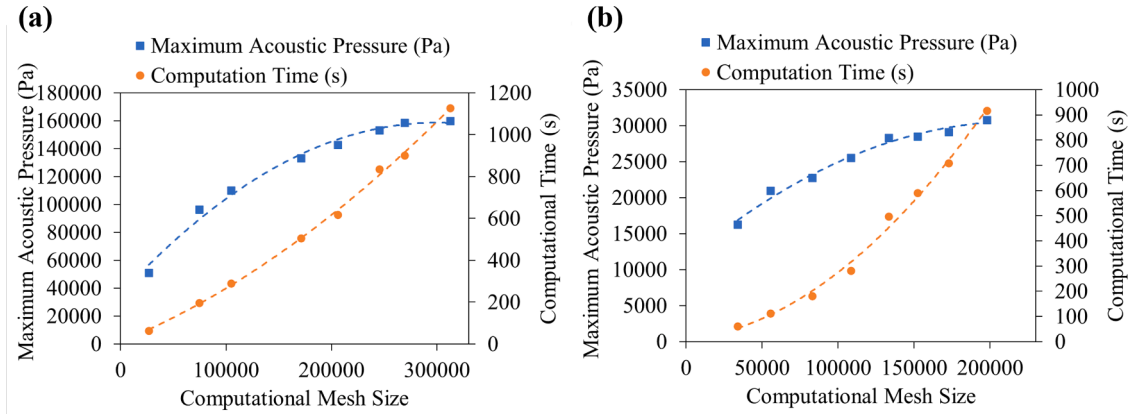


Fig. 3. Mesh dependency analysis for the (a) rectangular, and (b) circular geometry of the capillary tube.

$$\nabla \cdot \sigma + F_s = 0 \quad (11)$$

$$\varepsilon = \frac{1}{2} [\nabla U_s + (\nabla U_s)^T] \quad (12)$$

where σ is the stress tensor, E is called Young's modulus, ε is the strain tensor, F_s is the load per unit volume which in this system is caused by wave propagation in the fluid, and U_s is the solid displacement vector [74]. Free surface boundary conditions were applied to all surfaces and interfaces.

To accurately predict the behaviours of the whole three-dimensional system, it is important to correctly model what happens at the fluid-solid interfaces, where the acoustic field inside the water causes a large pressure on the glass capillary tubes and the vibration of the capillary tubes affects the water and the pressure field inside. In these acousto-fluidic systems, the acoustic waves propagate from the SAW device to the $\sim 1.0 \mu\text{L}$ droplet under the glass tube. Then the acoustic energy is transferred from the droplet to the capillary tube and causes vibrations of the solid surfaces, which in turn causes the propagation of sound waves into the water inside the capillary tubes. Thus, to simulate the fluid-solid interfaces, two-way couplings were employed between the water droplet and the capillary tube, and between the capillary tube and the water inside. This method correctly models how the acoustic field inside the fluid exerts a pressure on the capillary tube and how the vibration of the capillary tube (i.e. the structural acceleration) influences the fluid [74].

Simulation was performed using the commercial software package COMSOL Multiphysics (5.6) which is a finite element method (FEM)-based software package. Discretisation of the governing equations was performed using the FEM, and Newton's iterative method was used to solve the system of equations resulted from the discretisation. Initial values of the unknown variables were chosen to update the coefficients matrix of the governing equation system and then solve the system of

equations for the next step values of the unknown variables. This procedure was repeated until the difference between two consecutive values (i.e. the residual) was small enough depending on the simulation type. Here, all the solutions were converged with 10^{-6} criteria for the residual [74].

In order to validate the numerical model, the simulation results of the distances between the pressure node lines inside a rectangular glass capillary tube placed with 0° and 45° angles relative to the direction of the IDTs were compared with the data gathered from the experiments with the same conditions. Fig. 4 compares the distances between the pressure node lines obtained from both experimental and numerical studies for a rectangular glass capillary tube placed with 0° and 45° angles relative to the direction of the IDTs. The error bars were calculated based on the standard deviation of the line distance data measured for five different line patterns. It can be observed from Fig. 4 that the numerical model overestimates the line distance values by $\sim 2\%$ compared to the experimental data. Thus we can conclude that the simulation results have good agreements with the experimental ones. This numerical modelling method was previously shown to be capable of presenting the acoustic pressure field with a reasonable accuracy [49,50,60,75].

4. Results and Discussions

4.1. Particle Patterning inside Rectangular Glass Capillary Tube

The experimental results of particle patterns inside a rectangular glass capillary tube (dimensions: $3.5 \text{ mm} \times 0.8 \text{ mm}$) placed at different angles with respect to the alignment of the IDTs are presented in Fig. 5. In these cases, there is no flow of liquid. When the rectangular glass tube is parallel to the IDTs (Fig. 5(a)), the particle pattern lines are parallel to the IDTs. When the rectangular glass tube is at an angle of β (shown in Fig. 5(b) 15° , 4(c) 30° , 4(d) 45° , 4(e) 60° , 4(f) 75° and 4(g) 90°) with

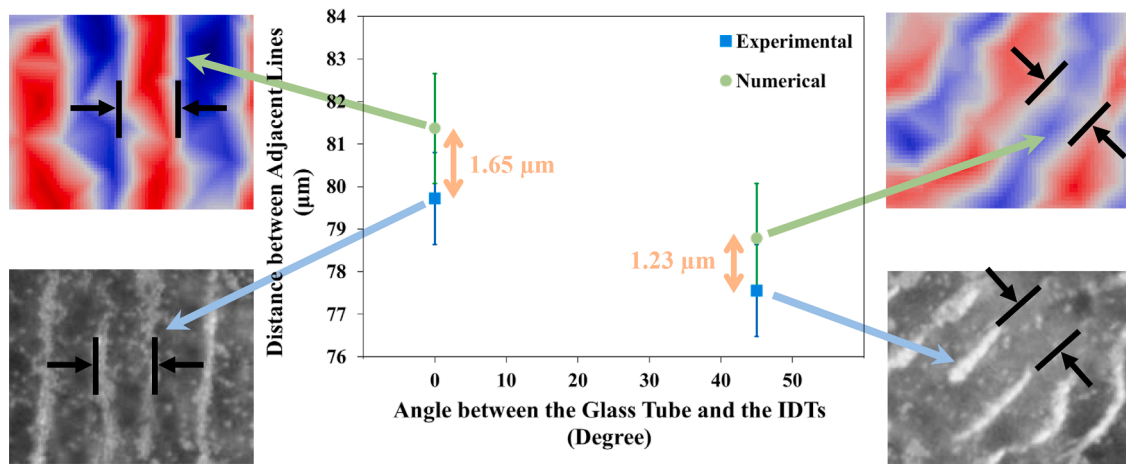


Fig. 4. Validation of the numerical model by comparing the distances between the pressure node lines inside a rectangular glass capillary tube placed with 0° and 45° angles relative to the direction of the IDTs.

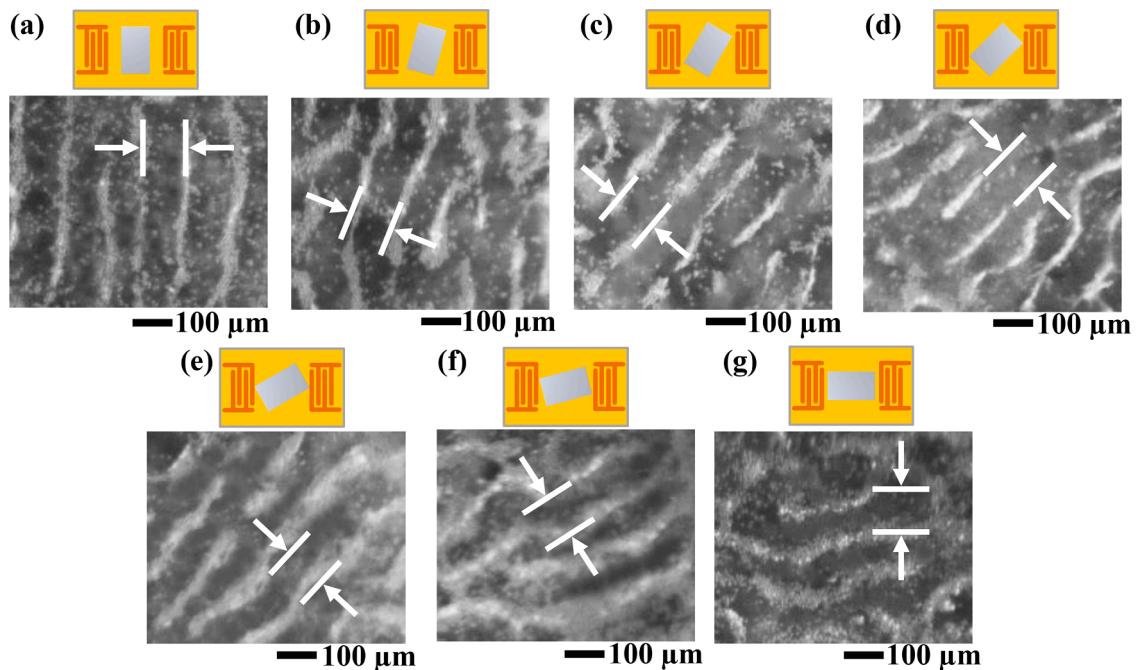


Fig. 5. Particle patterning inside the rectangular glass capillary tube ($3.5 \text{ mm} \times 0.8 \text{ mm}$) placed (a) parallel, with (b) 15° , (c) 30° , (d) 45° , (e) 60° , (f) 75° and (g) 90° incline angle relative to the IDTs, experimental data from top view shows particles patterning parallel to the tube walls with 13.12 MHz frequency.

respect to the alignment of the IDTs, the patterned lines of particles are also at an angle which is nearly the same as β to the IDTs (i.e., parallel to the tube walls).

The particles show the similar patterning behaviours in experiments using another type of rectangular glass capillary tube with a dimension of $4.5 \text{ mm} \times 1.0 \text{ mm}$, and the results are shown in Fig. S-1 in the supplementary information. We also observed accumulation of particles into a checker-board pattern, which are normally formed at the bottom of the tubes (see Fig. S-1 and S-2 in supplementary information).

The above experimental results shown in Fig. 5, Fig. S-1, and S-2 clearly show that there are two types of particle patterning phenomena. Fig. 6(a) shows the schematic mechanisms of wave and pattern formations. The first type of particle patterning is the line patterns parallel to the rectangular shape glass tube walls which is caused by the standing wave field inside the rectangular glass tube (see Fig. 6(a)). This is formed due to propagation of the acoustic waves into the glass tube and their reflection from the tube walls. Particles were also observed to form

checker-board patterns similar to those caused by the Lamb waves [76, 77] (see Fig. S-1 and S-2 in supplementary information). These patterns are normally formed at the bottom of the rectangular glass tube, because the SAWs from the substrate are transferred into the glass tube, forming Lamb waves at the bottom wall of the tube due to the superstrate effect [78].

Fig. 6(b) to (d) show the simulation results of the acoustic pressure fields inside the liquid when the angle β is equal to (a) 0° , (b) 45° , and (c) 90° and from (1) cross-sectional and (2) top views. From Fig. 6(b-1), (c-1) and (d-1) and (d-1), the pressure node lines are either vertical or parallel to the side walls of the rectangular capillary tubes for 0° , 45° , and 90° , respectively (see Fig. 6(b-1), (c-1) and (d-1)). For $\beta = 0^\circ$, by comparing Fig. 5(a) and Fig. 6(b-2), the pattern lines are parallel to the side walls of the rectangular capillary tube from both the experimental and simulation results (see Fig. 6(b-2)). Comparing Fig. 5(d) with Fig. 6(c-2) for $\beta = 45^\circ$ and Fig. 5(g) with Fig. 6(d-2) for $\beta = 90^\circ$, we can observe that as the angle between the directions of glass tube and the IDTs increases, the

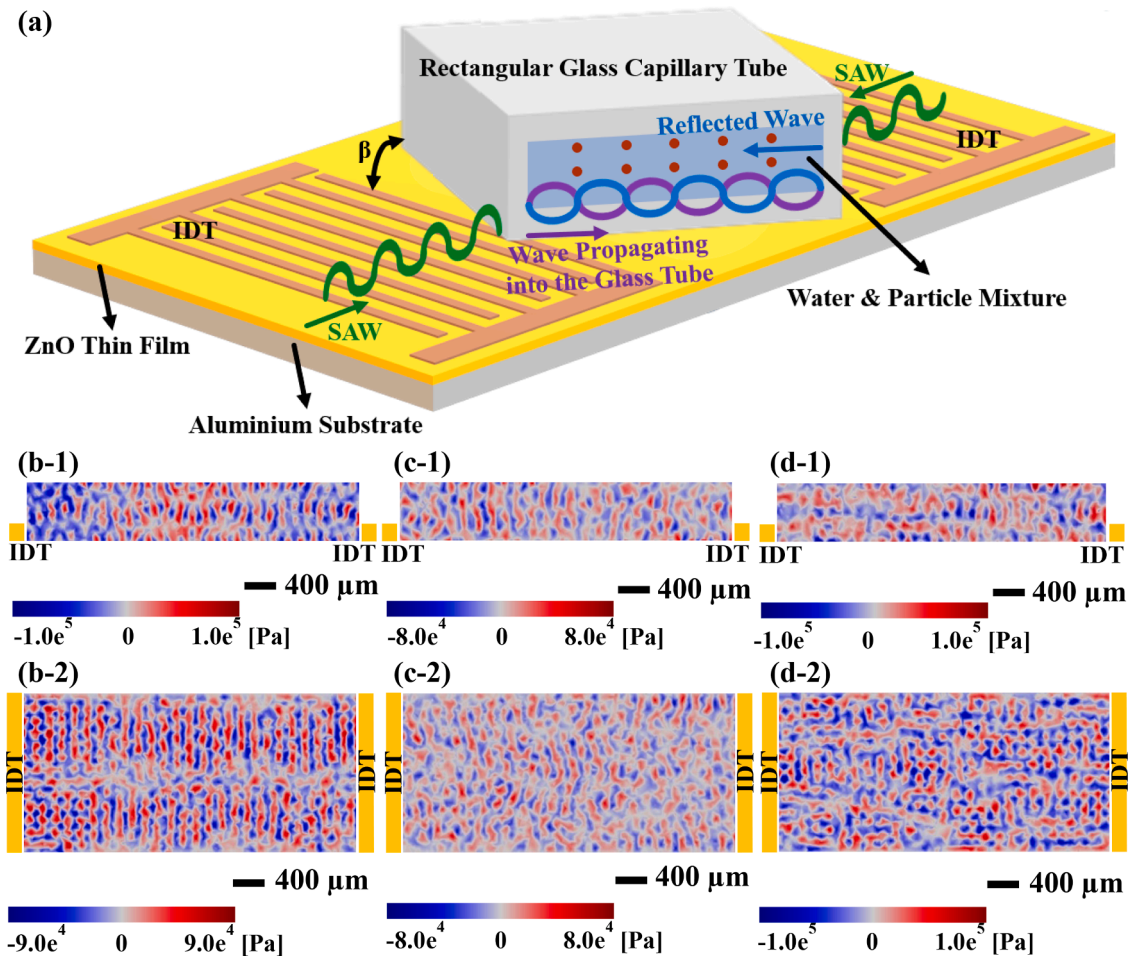


Fig. 6. (a) Schematic of the particle patterning inside rectangular glass capillary tube resulted from different wave formations inside the glass. The simulation results of the acoustic pressure field (Pa) inside the water for a capillary tube placed (b) parallel, with (c) 45°, and (d) 90° incline angle relative to the IDTs, (1) cross-sectional and (2) top view.

pattern lines remain perpendicular to the side walls of the tube from both the simulation and experimental results (see Fig. 6(c-2) and (d-2)). The simulation results show good agreements with those from the experiments.

4.2. Particle Patterning inside Circular Glass Capillary Tube

Fig. 7 shows the images of particle patterns that are generated inside the circular glass capillary tubes placed at different angles compared to the direction of the IDTs. When the circular glass tube is at an angle β equal to (a) 0°, (b) 30° and (c) 45° compared to the direction of the IDTs, the pattern lines of particles are also at an angle β to the IDTs (parallel to the tube walls) near the bottom of the tube (see Fig. 7(a-1), (b-1) and (c-1)). However, at the middle of the tubes with the above different angles (see Fig. 7(a-2), (b-2) and (c-2)), the pattern lines of particles are perpendicular to the tube walls (i.e., at an angle which is equal to $90^\circ - \beta$ to that of the IDTs). For a circular glass tube which is placed with an angle β equal to 60° compared to the IDTs, the pattern lines are also perpendicular to the tube walls (see in Fig. 7(d)). When the circular glass tube is placed perpendicular to the IDTs, the pattern lines are parallel to the IDTs and perpendicular to the tube walls (Fig. 7(e)).

It can be seen from Fig. 7 that the pattern lines which are parallel to the tube walls are relatively shorter and have a relatively larger distance between them (e.g., Fig. 7(b-1)), whereas the particle pattern lines which are perpendicular to the tube walls are relatively longer with smaller distances between them (e.g., Fig. 7(b-2)).

The above experimental results of particle patterns inside the

circular glass tubes (Fig. 7) clearly show that there are two different phenomena of particle patterning. The first one is that the pattern lines are parallel to the glass tube direction, and the second one is that the pattern lines are perpendicular to the tube direction. Both of these patterns are formed because the SAW energy from the substrate is transferred into the circular glass tube from each side which results in the generation of a complicated acoustic wave field inside the circular glass tube.

Fig. 8(a) presents a schematic illustration of the acoustic wave formation inside the circular glass tube. Fig. 8(b) to (d) show simulation results of the acoustic pressure fields inside the water for a circular capillary tube which is placed at (a) 0°, (b) 45°, and (c) 90° and from (1) cross-sectional view, and top view (2) near the bottom, and (3) at the middle of the glass tube, respectively. The simulation results show good agreements with experimental ones. When the waves propagate from the SAW device into the glass tube, a standing acoustic wave forms in the glass tube. This acoustic wave then transfers its energy into the water which will cause the patterning of the particles (see Fig. 8(a)).

For $\beta = 0^\circ$, by comparing Fig. 8(b-2) and 7(a-1), both the experimental and simulation results show that there are patterned lines at the bottom of the tube, which are parallel to the direction of the capillary tube. Whereas at the middle of the tube (see Fig. 8(b-3) and (c-3)), the standing waves, which propagate around the circular cross-section of the glass tube but perpendicular to the direction of the tube, cause that the pressure node lines are formed perpendicular to the tube walls. Both Fig. 8(b-3) and Fig. 7(a-2), which are the simulation and experimental results, show that the patterned lines are perpendicular to the direction

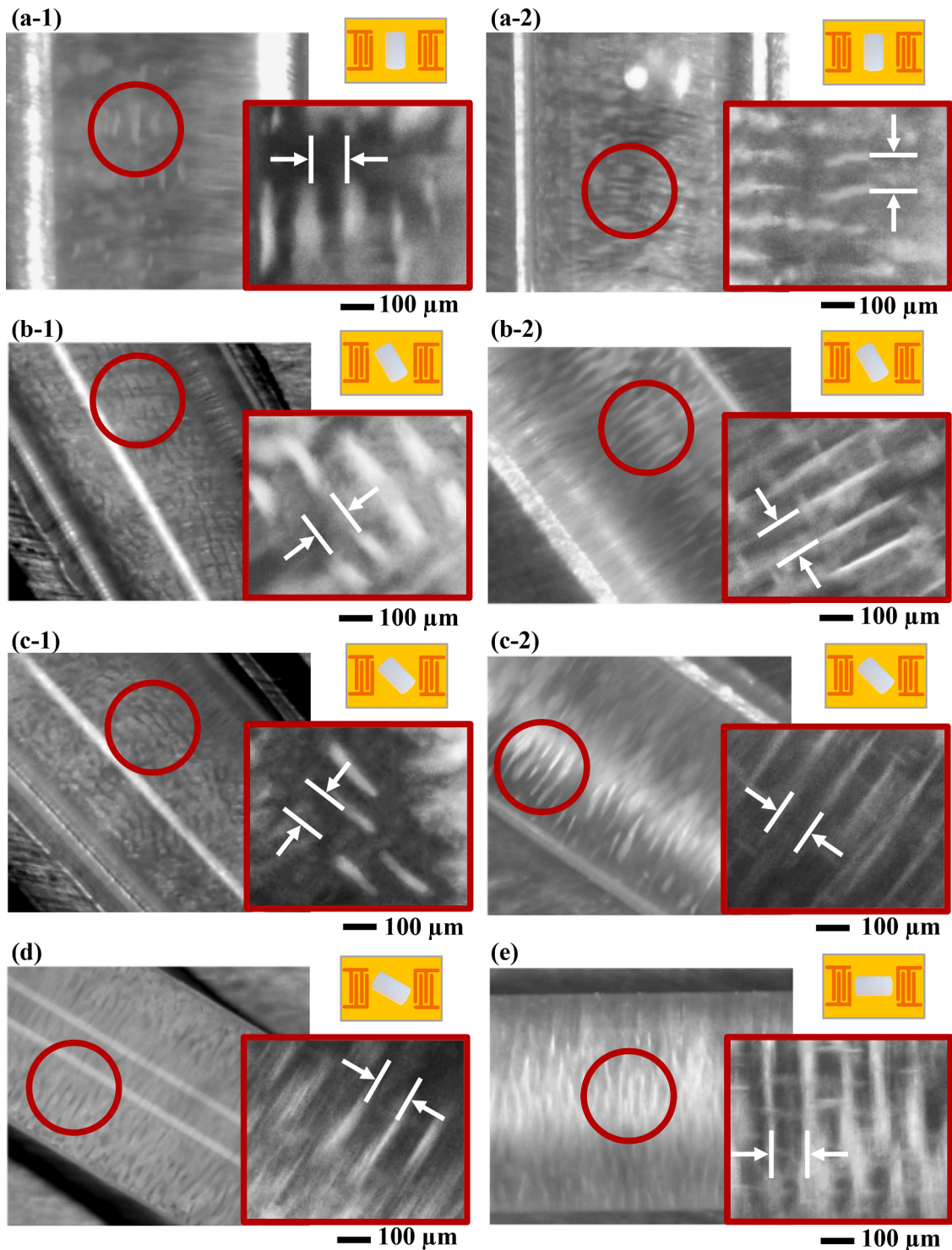


Fig. 7. Particle patterning inside the circular glass capillary tube (1 mm diameter) placed (a) parallel, with (b) 30°, (c) 45°, (d) 60° and (e) 90° incline angle relative to the IDTs, experimental data from top view shows particle patterning (1) parallel and (2) perpendicular to the tube walls, with 13.12 MHz frequency.

of the tube occurring at the middle height of the tube.

For $\beta \leq 45^\circ$, near the bottom of the tube (see Fig. 8(b-2) and (c-2)), the waves that propagate into the water generate a standing wave along the direction of the tube. This results in the pressure nodes to be parallel to the tube direction, thus causing the particles parallel to the glass tube direction.

Whereas for $\beta > 45^\circ$, a standing wave is generated perpendicular to the direction of the tube along the whole depth of tubes and the particles are patterned vertically to the tube walls. Comparing Fig. 8(d-2) and (d-

3) with Fig. 7(g-2), it can be observed that pattern lines obtained from both simulation and experimental results are perpendicular to the direction of tube walls for the whole depth of the tube.

Fig. 9 compares the estimated average values of (a) the distances between the particle line patterns inside (1) rectangular; and (2) circular tubes from both experiments and simulations; and (b) line pattern angles regarding the direction of the IDTs. It can be seen from Fig. 9(a-1) and (a-2) that for the circular tube, the particle pattern lines which are parallel to the tube walls have a relatively larger distance between them,

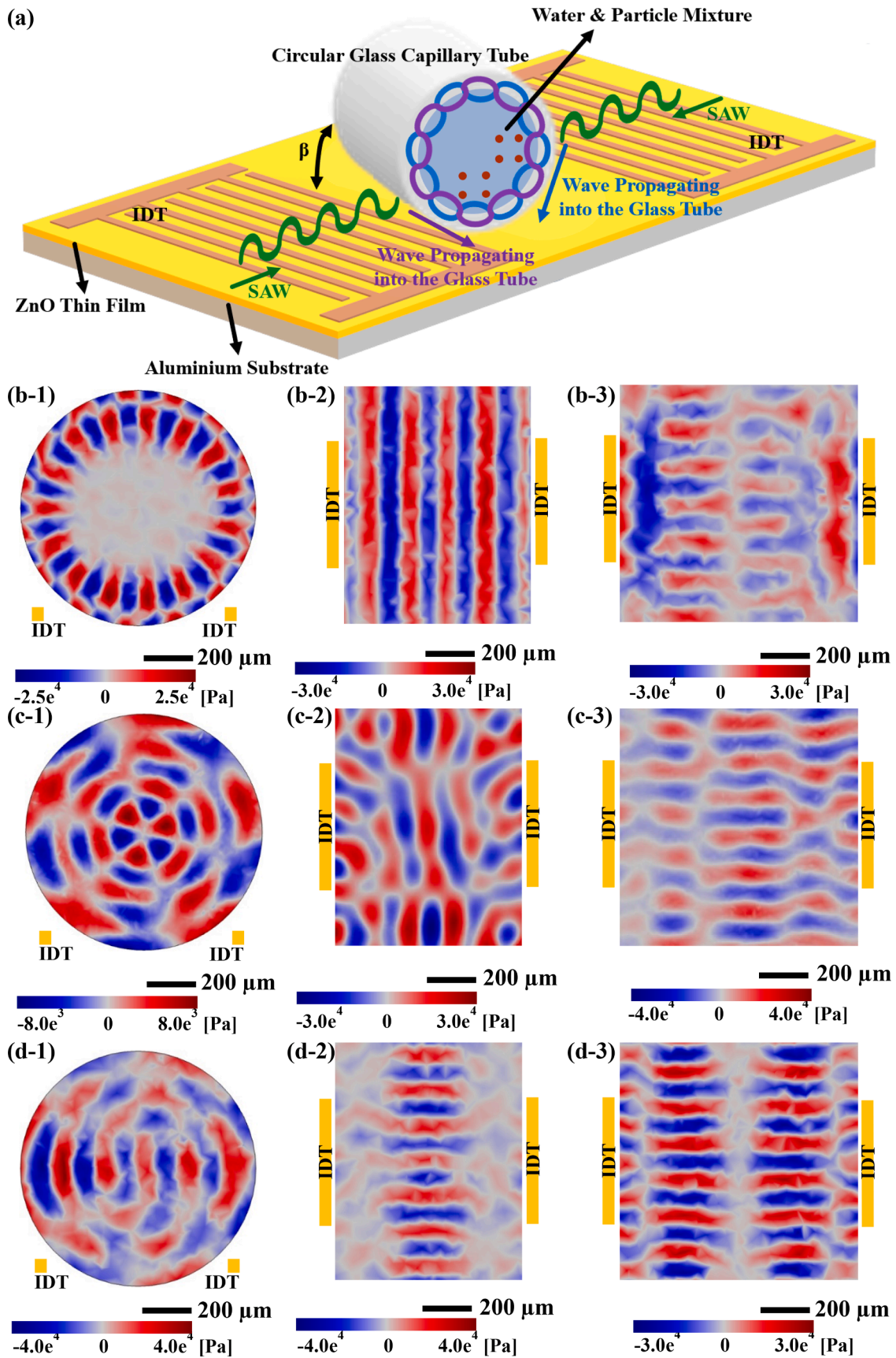


Fig. 8. (a) Schematic of the particle patterning inside circular glass capillary tube resulted from different wave formations inside the glass. The simulation results of the acoustic pressure field (Pa) inside the water for a capillary tube placed (b) parallel, with (c) 45°, and (d) 90° incline angle relative to the IDTs, (1) the cross-sectional view, (2) top view at the bottom of the tube and (3) top view at the middle of the tube.

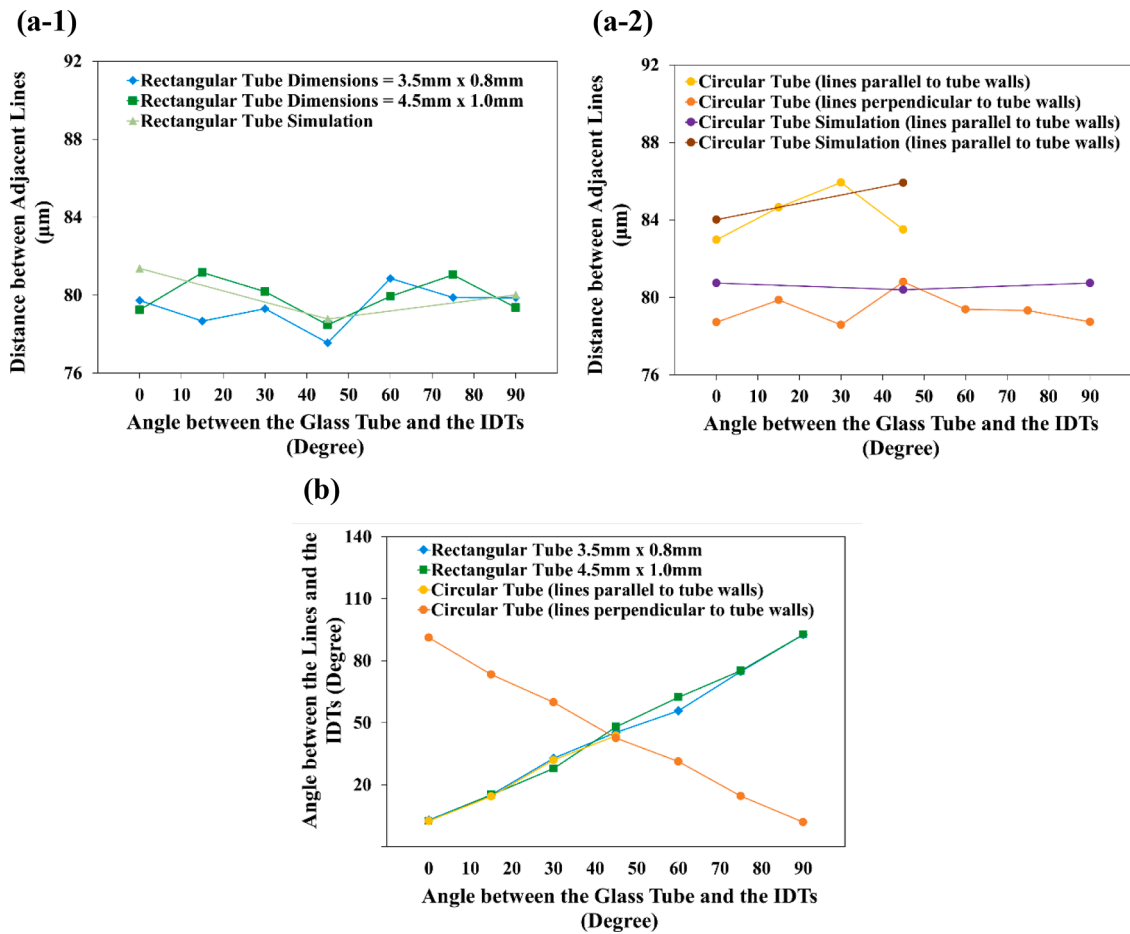


Fig. 9. Comparison of (a) the distance between two adjacent patterns inside (1) rectangular and (2) circular glass capillary tubes and (b) the angle between the lines and the IDTs for circular and rectangular glass tubes with 13.12 MHz frequency.

compared to the particle pattern lines which are perpendicular to the tube walls. In addition, the distances between the particle pattern lines inside the rectangular tubes is closer to the distances between particle pattern lines that are perpendicular to the circular tube walls (see Fig. 9 (a-1) and (a-2)). These can be verified from the simulation results as well (see Fig. 9(a-1) and (a-2)). One reason for this difference is attributed to the radial formation of the pressure nodes in the cross-section of the circular tube. This results in the distance between the pressure node lines to gradually increase towards the bottom of the tube compared to the middle height of the capillary tube. The simulations results show good agreements with the experimental data. Fig. 9(b) shows the estimated angles between the particle line patterns inside the glass tubes and the direction of the IDTs. The results clearly indicate that, for the rectangular tubes, the particle pattern lines are parallel to the tube walls. Whereas for the circular tube, the line patterns of particles are either parallel to the glass tube direction or perpendicular to it, depending on the position of the particles along the height of the tube.

4.3. Particle Patterning inside Glass Capillary Tubes with Continuous Fluid Flow

Particles were further patterned inside rectangular (dimensions: 2.3 mm × 0.5 mm) and circular glass capillary tubes with various fluid flow rates. The obtained experimental results are shown in Fig. 10 and 11, respectively. Figure 10 shows that the particles are patterned and flow in lines parallel to the walls of the rectangular glass tubes, for all the cases with the incline angles relative to the IDTs of (a) 0°, (b) 30°, (c) 60°, and (d) 90°, with different flow rates of (1) 0.2 μL/s, (2) 0.1 μL/s, (3) 0.05 μL/s, and (4) 0.01 μL/s, respectively. When the flow velocity is large

enough (e.g., Fig. 10(a-1)), the pattern lines which are parallel to the tube direction (also flow direction) are smoothed and enhanced. Whereas the previously observed checker-board-type patterns are mostly removed due to the liquid flow effect. Decreasing the flow rate gradually from 0.2 μL/s (e.g., Fig. 10(a-1)) to 0.01 μL/s (e.g., Fig. 10(a-4)) will cause the line patterns of particles to become distorted, and then finally change into the checker-board-like patterns. As explained previously, these patterns are caused by the Lamb waves [76,77], which are generated and propagated at the bottom wall of the tube due to the superstrate effect [78].

Fig. 11 shows the experimentally obtained images of particle patterns inside the circular glass capillary tube for the different inclined angles relative to the IDTs of (a) 0°, (b) 30°, (c) 45°, (d) 60°, and (e) 90°, with flow rate of (1) 0.2 μL/s, (2) 0.1 μL/s, (3) 0.05 μL/s, and (4) 0.01 μL/s, respectively. With an increased flow rate (e.g., Fig. 11(a-1)), the pattern lines which are perpendicular to the tube direction are removed due to the liquid flow and only the pattern lines which are parallel to the tube direction (also flow direction) remain and form smooth lines. When the flow rate is decreased (e.g., Fig. 11(a-4)), the particle pattern lines gradually become curved and distorted.

Fig. 12 further compares the estimated measured average distances between the particle line patterns inside (a) rectangular and (b) circular tubes with various flow rates. Fig. 12(a) shows that the average distance between the adjacent particle pattern lines in the rectangular glass tube is nearly equal to the half of the wavelength in water, which is not changed by changing the flow rate. Comparing Fig. 12(a) and (b), it can be seen that for the circular glass tube, its distance between adjacent particle pattern lines is slightly larger than that in the rectangular case. However, this insignificant difference could be caused by the radial

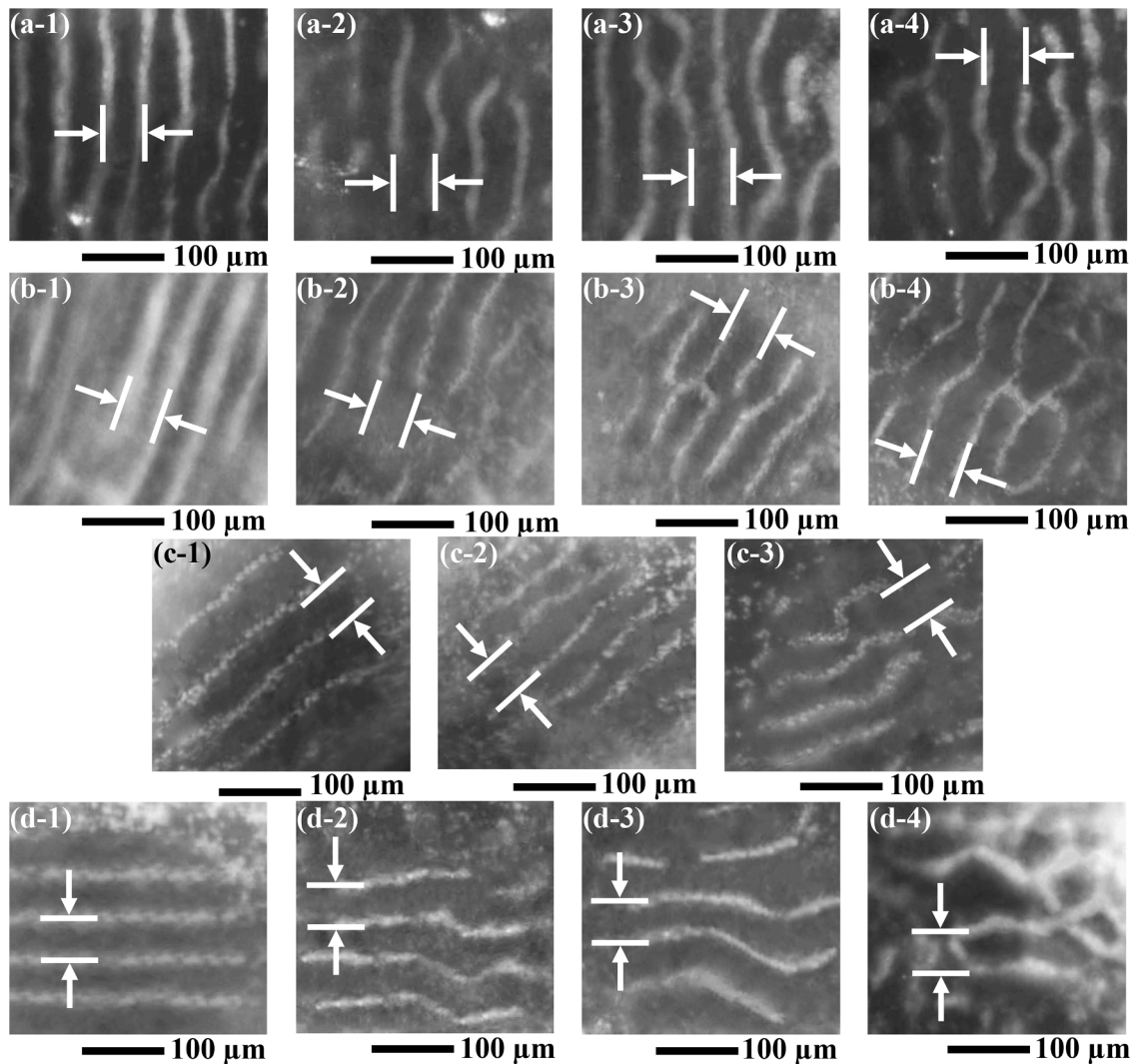


Fig. 10. Particle patterning in inside the rectangular glass capillary tube (2.3 mm x 0.5 mm) placed (a) parallel, with (b) 30°, (c) 60°, and (d) 90° incline angle relative to the IDTs, in continuous flow setup with flow rate of (1) 0.2 $\mu\text{L/s}$, (2) 0.1 $\mu\text{L/s}$, (3) 0.05 $\mu\text{L/s}$, and (4) 0.01 $\mu\text{L/s}$; experimental data from top view and with 13.12 MHz frequency.

formation of the pressure nodes in the cross-section of the circular tube as previously discussed.

5. Discussions

In the previous section, it was presented that due to the acoustic radiation forces the microparticles form linear patterns inside the capillary tubes. The cross-section of the capillary tubes has shown a significant effect on the particle patterning phenomena. Capillary tubes with rectangular cross-sections show similar phenomena compared to the traditional rectangular microchannels. For these capillary tubes, an acoustic standing wave field is formed inside the tube with its pressure node lines parallel to the tube walls, irrelevant to the tube position along with the IDTs. This results in the microparticles patterned in lines parallel to the side walls of tubes.

For capillary tubes with circular cross-sections, the acoustic standing wave field generated inside the tube is more complicated. The formation of the acoustic pressure node lines inside these capillary tubes is dependent on the position along the height of the cross-section. At the bottom of the tube, the pressure node lines are parallel to the tube direction, whereas at the middle height of the tube, the pressure node lines are perpendicular to the tube direction as the waves propagate around the circular cross-section of the tube. This results in particle alignment at

the bottom and middle height of the tube to be parallel and perpendicular to the tube walls, respectively.

Choosing a proper combination of SAW device properties (frequency, wavelength, etc.), capillary tube geometry (shape, dimensions, thickness, etc.) and flow parameters will result in the formation of a desirable number of pressure node lines inside the capillary tube. Fig. 13 (a) and (b) show the simulation results of acoustic pressure fields inside a rectangular glass tube with dimensions of 0.2 mm \times 0.2 mm and a circular glass tube with a diameter of 0.15 mm from (1) cross-sectional and (2) top views, respectively. It can be seen that in these two cases, there is a single pressure node formed at the centre of the capillary tube where the particles/cells will be patterned. A proper combination of the acoustic frequency (or wavelength) with capillary tube geometry results in the generation of a desirable number of pressure node lines inside the capillary tube. This can be used in the continuous flow systems to focus, pattern and separate microparticles/cells. In brief, these glass capillary tubes show great potentials to be used in acoustofluidics since they are low-cost, disposable, and simple to integrate in the setups.

Using capillary bridge channels integrated with flexible or bendable thin film SAW devices offers great advantages for acoustofluidic applications. Our flexible SAW devices can be bent into different shapes to be conformal to various types of surfaces. They can wrap around the capillary tubes with various geometries and enhance the concentration

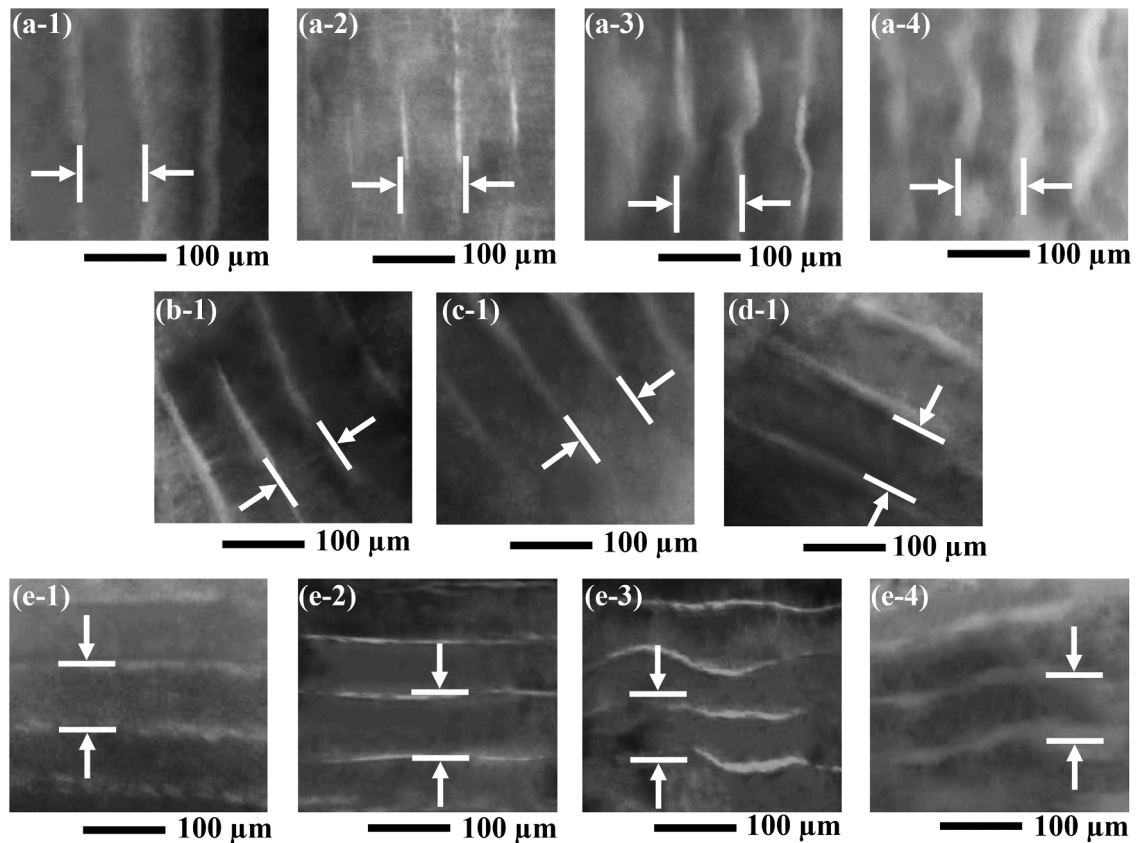


Fig. 11. Particle patterning in inside the circular glass capillary tube (1.00 mm diameter) placed (a) parallel, with (b) 30°, (c) 45°, (d) 60°, and (e) 90° incline angle relative to the IDTs, in continuous flow setup with flow rate of (1) 0.2 $\mu\text{L/s}$, (2) 0.1 $\mu\text{L/s}$, (3) 0.05 $\mu\text{L/s}$, and (4) 0.01 $\mu\text{L/s}$; experimental data from top view and with 13.12 MHz frequency.

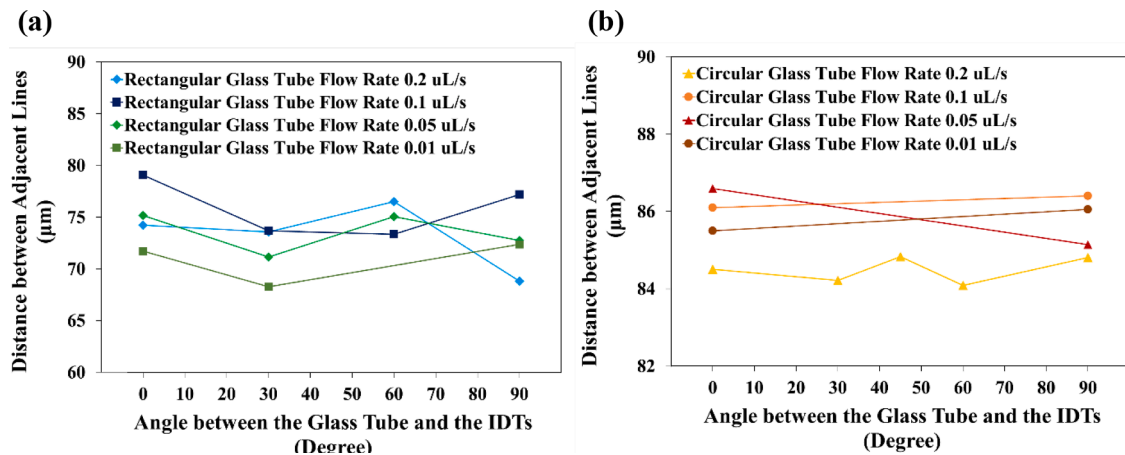


Fig. 12. Comparison of the distance between two adjacent patterns inside glass capillary tubes for (a) rectangular and (b) circular glass tubes with 13.12 MHz frequency.

effects of the acoustic waves. These flexible thin film SAW devices can be easily integrated with other acoustofluidic or sensing technologies, as well as the fabrication processes of the microelectronic and lab-on-chips, with a great potential for applications in flexible microfluidic platforms, body conforming wearable devices, flexible sensors and electronics.

6. Conclusions

In this paper, we systematically investigated the patterning and alignment of microparticles inside glass capillary tubes using a thin film

SAW device. We studied the effects of different tube cross-sections, and tube's positioning angles regarding to the directions of the IDTs with and without liquid flow. For the rectangular glass capillary tubes, the particle pattern lines are parallel to the tube walls for each relative angle, which is due to the generation of the standing wave field inside the rectangular tube. For the circular glass capillary tubes, different patterns of particles can be observed which depends on their position along the tube's height. At the bottom of the tube, the particle pattern lines are parallel to the tube direction for all the angles in relation to the IDTs, mainly because the acoustic waves propagate into the water and form a

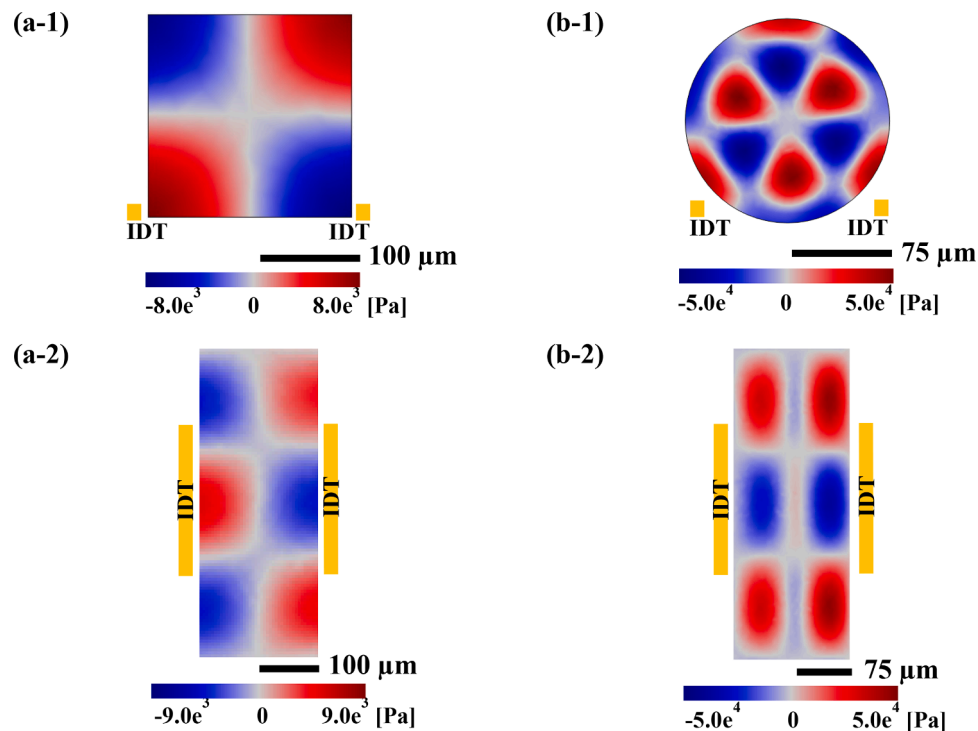


Fig. 13. Simulation results of the acoustic pressure field (Pa) inside the capillary tubes with (a) rectangular and (b) circular cross-section from (1) cross-sectional and (2) top views with 13.12 MHz frequency.

standing wave along the direction of the circular tube. Whereas, near the middle height of the tube, the patterned lines of particle are perpendicular to the tube direction at each angle regarding to the IDTs' directions. This is due to the propagation of the standing wave around the circular cross-section of the tube with the pressure node line becoming perpendicular to the tube direction at the middle height of the tube. The continuous flow inside all the glass tubes causes the particles to form smooth line patterns which are parallel to the direction of the flow for all the angles.

CRediT authorship contribution statement

Sadaf Maramizonouz: Conceptualization, Data curation, Formal analysis, Investigation, Methodology, Validation, Visualization, Writing – original draft, Writing – review & editing. **Changfeng Jia:** Investigation. **Mohammad Rahmati:** Funding acquisition, Project administration, Resources, Supervision, Writing – review & editing. **Tengfei Zheng:** Funding acquisition, Resources, Writing – review & editing. **Qiang Liu:** Funding acquisition, Resources, Writing – review & editing. **Hamdi Torun:** Funding acquisition, Resources, Writing – review & editing. **Qiang Wu:** Funding acquisition, Resources, Writing – review & editing. **YongQing Fu:** Conceptualization, Funding acquisition, Methodology, Resources, Supervision, Project administration, Writing – review & editing.

Declaration of Competing Interest

The authors declare that they have no known competing financial interests or personal relationships that could have appeared to influence the work reported in this paper.

Acknowledgments

This work was supported by the Engineering and Physical Sciences Research Council of UK (EPSRC EP/P018998/1), UK Fluidic Network Special Interest Group of Acoustofluidics (EP/N032861/1),

International Exchange Grant (IEC/NSFC/201078) through Royal Society and the National Natural Science Foundation of China, and EPSRC NetworkPlus in Digitalised Surface Manufacturing (EP/S036180/1).

Supplementary materials

Supplementary material associated with this article can be found, in the online version, at doi:10.1016/j.ijmecs.2021.106893.

References

- [1] Huang TJ. Acoustofluidics: Merging Acoustics and Microfluidics for Biomedical Applications. *The Journal of the Acoustical Society of America* 2019;145(3):1786. <https://doi.org/10.1121/1.5101531>. 17862019/03/01.
- [2] Friend J, Yeo LY. Microscale Acoustofluidics: Microfluidics Driven via Acoustics and Ultrasonics. *Reviews of Modern Physics* 2011;83(2):647–704. <https://doi.org/10.1103/RevModPhys.83.647>. 06/20/.
- [3] Franke T, Braunnmuller S, Schmid L, Wixforth A, Weitz DA. Surface Acoustic Wave Actuated Cell Sorting (SAWACS). *Lab on a chip* 2010;10(6):789–94. <https://doi.org/10.1039/b915522h>. Mar 21.
- [4] Schmid L, Weitz DA, Franke T. Sorting Drops and Cells with Acoustics: Acoustic Microfluidic Fluorescence-Activated Cell Sorter. *Lab on a chip* 2014;14(19):3710–8. <https://doi.org/10.1039/c4lc00588k>.
- [5] Wang K, Zhou W, Lin Z, Cai F, Li F, Wu J-r, Meng L, Niu L, Zheng H. Sorting of Tumour Cells in a Microfluidic Device by Multi-Stage Surface Acoustic Waves. *Sensors and Actuators B: Chemical* 2017;258:1174–83. <https://doi.org/10.1016/j.snb.2017.12.013>.
- [6] Wu M, Ozelik A, Rufo J, Wang Z, Fang R, Huang TJ. Acoustofluidic Separation of Cells and Particles. *Microsystems & Nanoengineering* 2019;5(1):32. <https://doi.org/10.1038/s41378-019-0064-3>. 2019/06/03.
- [7] Petersson F, Nilsson A, Holm C, Jonsson H, Laurell T. Separation of Lipids from Blood Utilizing Ultrasonic Standing Waves in Microfluidic Channels. in eng *The Analyst* 2004;129(10):938–43. <https://doi.org/10.1039/b409139f>. Oct.
- [8] Ai Y, Marrone BL. Separation of Biological Cells in a Microfluidic Device Using Surface Acoustic Waves (SAWs). in *SPIE MOEMS-MEMS 2014*;8976:7. SPIE.
- [9] Nam J, Lim H, Kim D, Shin S. Separation of Platelets from Whole Blood Using Standing Surface Acoustic Waves in a Microchannel. in eng *Lab on a chip* 2011;11(19):3361–4. <https://doi.org/10.1039/c1lc20346k>. Oct 7.
- [10] Xie Y, Bachman H, Huang TJ. Acoustofluidic Methods in Cell Analysis. *TrAC Trends in Analytical Chemistry* 2019;117:280–90.
- [11] Whitesides GM. The Origins and the Future of Microfluidics. *Nature* 2006;442(7101):368. <https://doi.org/10.1038/nature05058>.
- [12] Fu YQ, Luo JK, Nguyen NT, Walton AJ, Flewitt AJ, Zu XT, Li Y, McHale G, Mathews A, Iborra E, Du H, Milne WI. Advances in Piezoelectric Thin Films for

- Acoustic Biosensors, Acoustofluidics and Lab-on-Chip Applications. *Progress in Materials Science* 2017;89:31–91. <https://doi.org/10.1016/j.pmatsci.2017.04.006>.
- [13] Conacher W, Zhang N, Huang A, Mei J, Zhang S, Gopesh T, Friend J. *Micro/Nano Acoustofluidics: Materials, Phenomena, Design, Devices and Applications*. Lab on a chip 2018;18(14):1952–96.
- [14] Li P, Huang TJ. Applications of Acoustofluidics in Bioanalytical Chemistry. *Analytical chemistry* 2018;91(11):757–67. <https://doi.org/10.1021/acs.analchem.8b03786>.
- [15] Sato K, Kamada S, Minami K. Development of Microstretching Device to Evaluate Cell Membrane Strain Field Around Sensing Point of Mechanical Stimuli. *International Journal of Mechanical Sciences* 2010;52(2):251–6.
- [16] Hong T-F, Ju W-J, Wu M-C, Tai C-H, Tsai C-H, Fu L-M. Rapid Prototyping of PMMA Microfluidic Chips Utilizing a CO₂ Laser. *Microfluidics and Nanofluidics* 2010;9(6):1125–33.
- [17] Liga A, Morton JA, Kersaudy-Kerhoas M. Safe and Cost-Effective Rapid-Prototyping of Multilayer PMMA Microfluidic Devices. *Microfluidics and Nanofluidics* 2016;20(12):1–12.
- [18] Nilsson A, Petersson F, Jonsson H, Laurell T. Acoustic Control of Suspended Particles in Micro Fluidic Chips. in *eng Lab on a chip* Apr 2004;4(2):131–5. <https://doi.org/10.1039/b313493h>.
- [19] Wang H, Liu Z, Shin DM, Chen ZG, Cho Y, Kim Y-J, Han A. A Continuous-Flow Acoustofluidic Cytometer for Single-Cell Mechanotyping. *Lab on a chip* 2019;19(3):387–93.
- [20] Raiton B, McLaughlan J, Harput S, Smith P, Cowell D, Freear S. The Capture of Flowing Microbubbles with an Ultrasonic Tap Using Acoustic Radiation Force. *Applied Physics Letters* 2012;101(4):044102.
- [21] Gralinski I, Raymond S, Alan T, Neild A. Continuous Flow Ultrasonic Particle Trapping in a Glass Capillary. *Journal of Applied Physics* 2014;115(5):054505.
- [22] O'Mahoney P, McDougall C, Glynne-Jones P, MacDonald M. Acoustic Trapping in Bubble-Bounded Micro-Cavities. *Optofluidics, Microfluidics and Nanofluidics* 2016;3(1).
- [23] Hammarström B, Evander M, Barbeau H, Bruzelius M, Larsson J, Laurell T, Nilsson J. Non-Contact Acoustic Cell Trapping in Disposable Glass Capillaries. *Lab on a chip* 2010;10(17):2251–7.
- [24] Hammarström B, Laurell T, Nilsson J. Seed Particle-Enabled Acoustic Trapping of Bacteria and Nanoparticles in Continuous Flow Systems. *Lab on a chip* 2012;12(21):4296–304.
- [25] Hammarström Br, Nilson B, Laurell T, Nilsson J, Ekström S. Acoustic Trapping for Bacteria Identification in Positive Blood Cultures with MALDI-TOF MS. *Analytical chemistry* 2014;86(21):10560–7.
- [26] Glynne-Jones P, Demore CE, Ye C, Qiu Y, Cochran S, Hill M. Array-Controlled Ultrasonic Manipulation of Particles in Planar Acoustic Resonator. *IEEE Transactions on Ultrasonics, Ferroelectrics, and Frequency Control* 2012;59(6):1258–66.
- [27] Fornell A, Johannesson C, Searle SS, Happstadia A, Nilsson J, Tenje M. An Acoustofluidic Platform for Non-Contact Trapping of Cell-Laden Hydrogel Droplets Compatible with Optical Microscopy. *Biomicrofluidics* 2019;13(4):044101.
- [28] Fornell A, Baasch T, Johannesson C, Nilsson J, Tenje M. Binary Acoustic Trapping in a Glass Capillary. *Journal of Physics D: Applied Physics* 2021;54(35):355401.
- [29] Goddard G, Martin JC, Graves SW, Kaduchak G. Ultrasonic Particle-Concentration for Sheathless Focusing of Particles for Analysis in a Flow Cytometer. *Cytometry Part A: The Journal of the International Society for Analytical Cytology* 2006;69(2):66–74.
- [30] Perfetti C, Iorio CS. Three-Dimensional Matrixlike Focusing of Microparticles in Flow through Minichannel Using Acoustic Standing Waves: An Experimental and Modeling Study. *Acoustical Science and Technology* 2016;37(5):221–30.
- [31] Galanzha EI, Viegas MG, Malinsky TI, Melerzanov AV, Juratli MA, Sarimollaoglu M, Nedosekin DA, Zharov VP. In Vivo Acoustic and Photoacoustic Focusing of Circulating Cells. *Scientific Reports* 2016;6(1):1–15.
- [32] Li Z, Li P, Xu J, Shao W, Yang C, Cui Y. Hydrodynamic Flow Cytometer Performance Enhancement by Two-Dimensional Acoustic Focusing. *Biomedical Microdevices* 2020;22(2):1–12.
- [33] González I, Andrés RR, Pinto A, Carreras P. Influence of Hydrodynamics and Hematocrit on Ultrasound-Induced Blood Plasmapheresis. *Micromachines* 2020;11(8):751.
- [34] Lei J, Cheng F, Li K, Guo Z. Two-Dimensional Concentration of Microparticles Using Bulk Acousto-Microfluidics. *Applied Physics Letters* 2020;116(3):033104.
- [35] Lei J, Cheng F, Li K, Liu G, Zhang Y, Guo Z, Zhang Y. Simultaneous Imaging and Manipulation of Microparticles in Horizontal and Vertical Planes of Microchannels Using a Single Objective Lens. *Applied Physics Letters* 2020;117(22):224101.
- [36] Lata JP, Guo F, Guo J, Huang PH, Yang J, Huang TJ. Surface Acoustic Waves Grant Superior Spatial Control of Cells Embedded in Hydrogel Fibers. *Advanced Materials* 2016;28(39):8632–8.
- [37] Guo F, Zhou W, Li P, Mao Z, Yennawar NH, French JB, Huang TJ. Precise Manipulation and Patterning of Protein Crystals for Macromolecular Crystallography Using Surface Acoustic Waves. *Small* 2015;11(23):2733–7.
- [38] Lei J, Glynne-Jones P, Hill M. Acoustic Streaming in the Transducer Plane in Ultrasonic Particle Manipulation Devices. *Lab on a chip* 2013;13(11):2133–43.
- [39] Koo K-i, Lenschof A, Huang LT, Laurell T. Acoustic Cell Patterning in Hydrogel for Three-Dimensional Cell Network Formation. *Micromachines* 2021;12(1):3.
- [40] Piyasena ME, Suthanthiraraj PPA, Applegate RW, Goumas AM, Woods TA, López GP, Graves SW. Multinode Acoustic Focusing for Parallel Flow Cytometry. *Analytical chemistry* 2012;84(4):1831–9. <https://doi.org/10.1021/ac200963n>.
- [41] Sobanski MA, Tucker CR, Thomas NE, Coakley WT. Sub-Micron Particle Manipulation in an Ultrasonic Standing Wave: Applications in Detection of Clinically Important Biomolecules. *Bioseparation* 2000;9(6):351–7.
- [42] Araz MK, Lee C-H, Lal A. Ultrasonic Separation in Microfluidic Capillaries. In: *IEEE Symposium on Ultrasonics*. 1; 2003. p. 1066–9. 2003IEEE.
- [43] Mishra P, Hill M, Glynne-Jones P. Deformation of Red Blood Cells Using Acoustic Radiation Forces. *Biomicrofluidics* 2014;8(3):034109.
- [44] Mao Z, Li P, Wu M, Bachman H, Mesyngier N, Guo X, Liu S, Costanzo F, Huang TJ. Enriching Nanoparticles via Acoustofluidics. *ACS Nano* 2017;11(1):603–12.
- [45] Xie Y, Rufo J, Zhong R, Rich J, Li P, Leong KW, Huang TJ. Microfluidic Isolation and Enrichment of Nanoparticles. *ACS Nano* 2020;14(12):16220–40.
- [46] Lisa G, Stefan R, Branka D-K, Ewald B. A New Ultrasonic-Based Cell Immobilization Technique. In: *Proceedings of Forum Acusticum*; 2002. p. 16–20. 09.
- [47] Sriputkiat Y, Zhou Y. Acoustic Manipulation of Microparticle in a Cylindrical Tube for 3D Printing. *Rapid Prototyping Journal* 2019.
- [48] Liu G, Lei J, Cheng F, Li K, Ji X, Huang Z, Guo Z. Ultrasonic Particle Manipulation in Glass Capillaries: A Concise Review. *Micromachines* 2021;12(8):876.
- [49] Gralinski I, Alan T, Neild A. Non-Contact Acoustic Trapping in Circular Cross-Section Glass Capillaries: A Numerical Study. *The Journal of the Acoustical Society of America* 2012;132(5):2978–87.
- [50] Ley MW, Bruus H. Three-Dimensional Numerical Modeling of Acoustic Trapping in Glass Capillaries. *Physical Review Applied* 2017;8(2):024020.
- [51] Bach JS, Bruus H. Theory of Acoustic Trapping of Microparticles in Capillary Tubes. *Physical Review E* 2020;101(2):023107.
- [52] Pushpa B, Sankar M, Mebarek-Oudina F. Buoyant Convective Flow and Heat Dissipation of Cu-H₂O Nanoliquids in an Annulus Through a Thin Baffle. *Journal of Nanofluids* 2021;10(2):292–304.
- [53] Sankar M, Jang B, Do Y. Numerical Study of Non-Darcy Natural Convection from Two Discrete Heat Sources in a Vertical Annulus. *Journal of Porous Media* 2014;17(5).
- [54] Girish N, Sankar M, Reddy K. Analysis of Fully Developed Mixed Convection in Open-Ended Annuli with Viscous Dissipation. *Journal of Thermal Analysis and Calorimetry* 2021;143(1):503–21.
- [55] Mebarek-Oudina F. Numerical Modeling of the Hydrodynamic Stability in Vertical Annulus with Heat Source of Different Lengths. *Engineering science and technology, an international journal* 2017;20(4):1324–33.
- [56] Tian R, Nie G, Liu J, Pan E, Wang Y. On Rayleigh Waves in a Piezoelectric Semiconductor Thin Film over an Elastic Half-space. *International Journal of Mechanical Sciences* 2021;106:565.
- [57] Nguyen N-T. Research Highlight Soft Microsystems - A Paradigm Shift in Engineering Small Systems. *Micro and Nanosystems* 2015;7(1):2–3. <https://doi.org/10.2174/187640290701150729123546.07/29>.
- [58] Tao R, Wang W, Luo J, Hasan SA, Torun H, Canelles-Pericas P, Zhou J, Xuan W, Cooke M, Gibson D. Thin Film Flexible/Bendable Acoustic Wave Devices: Evolution, Hybridization and Decoupling of Multiple Acoustic Wave Modes. *Surface and Coatings Technology* 2019;357:587–94.
- [59] Holmes DP, Tavakol B, Froehlicher G, Stone HA. Control and Manipulation of Microfluidic Flow via Elastic Deformations. *Soft Matter* 2013;9(29):7049–53.
- [60] Maramizonouz S, Tao X, Rahmati M, Jia C, Tao R, Torun H, Zheng T, Jin H, Dong S, Luo J. Flexible and Bendable Acoustofluidics for Particle and Cell Patterning. *International Journal of Mechanical Sciences* 2021;202:106536.
- [61] Fu YQ, Luo J, Du X, Flewitt A, Li Y, Marck G, Walton A, Milne W. Recent Developments on ZnO Films for Acoustic Wave Based Bio-Sensing and Microfluidic Applications: A Review. *Sensors and Actuators B: Chemical* 2010;143(2):606–19.
- [62] Ding X, Li P, Lin S-CS, Stratton ZS, Nama N, Guo F, Slotcavage D, Mao X, Shi J, Costanzo F, Huang TJ. Surface Acoustic Wave Microfluidics. *Lab on a chip* 2013;13(18):3626–49. <https://doi.org/10.1039/C3LC50361E>. 10.1039/C3LC50361E.
- [63] King LV. On The Acoustic Radiation Pressure on Spheres. *Proceedings of the Royal Society of London. Series A-Mathematical and Physical Sciences* 1934;147(861):212–40. <https://doi.org/10.1098/rspa.1934.0215>.
- [64] Yosioka K, Kawasima Y. Acoustic Radiation Pressure on a Compressible Sphere. *Acta Acustica united with Acustica* 1955;5(3):167–73.
- [65] Gorkov LP. On the Forces Acting on a Small Particle in an Acoustical Field in an Ideal Fluid. *Soviet Physics - Doklady* 1962;6:773–5.
- [66] Doinikov AA. Acoustic Radiation Pressure on a Rigid Sphere in a Viscous Fluid. *Proceedings of the Royal Society of London. Series A-Mathematical and Physical Sciences* 1931;447:447–66. <https://doi.org/10.1098/rspa.1994.0150>. 1994.
- [67] Doinikov AA. Acoustic Radiation Pressure on a Compressible Sphere in a Viscous Fluid. *Journal of Fluid Mechanics* 1994;267:1–22. <https://doi.org/10.1017/S0022112094001096>.
- [68] Settles M, Bruus H. Forces Acting on a Small Particle in an Acoustical Field in a Viscous Fluid. *Physical Review E* 2012;85(1):016327. <https://doi.org/10.1103/PhysRevE.85.016327>.
- [69] Liu S, Yang Y, Ni Z, Guo X, Luo L, Tu J, Zhang D, Zhang J. Investigation into the Effect of Acoustic Radiation Force and Acoustic Streaming on Particle Patterning in Acoustic Standing Wave Fields. *Sensors* 2017;17(7):1664. <https://doi.org/10.3390/s17071664> (Basel, Switzerland).
- [70] Doinikov AA. Acoustic Radiation Forces: Classical Theory and Recent Advances. *Recent Research Developments in Acoustics* 2003;1:39–67. ch. 3.
- [71] Crowe CT. *Multiphase Flow Handbook*. CRC press; 2005.
- [72] Crowe CT, Schwarzkopf JD, Sommerfeld M, Tsuji Y. *Multiphase Flows with Droplets and Particles*. CRC press; 2011.
- [73] Devendran C, Albrecht T, Brenker J, Alan T, Neild A. The Importance of Travelling Wave Components in Standing Surface Acoustic Wave (SSAW) Systems. *Lab on a chip* 2016;16(19):3756–66. <https://doi.org/10.1039/C6LC00798H>.

- [74] COMSOL. COMSOL User's Guide. 2018. 5.6 ed.
- [75] Maramizonouz S, Rahmati M, Link A, Franke T, Fu Y. Numerical and Experimental Studies of Acoustic Streaming Effects on Microparticles/Droplets in Microchannel Flow. *International Journal of Engineering Science* 2021;169:103563.
- [76] Rezk AR, Tan JK, Yeo LY. HYbrid Resonant Acoustics (HYDRA). *Advanced Materials* 2016;28(10):1970–5.
- [77] Azizi N, Saadatpour M, Mahzoon M. Analyzing First Symmetric and Antisymmetric Lamb Wave Modes in Functionally Graded Thick Plates by Using Spectral Plate Elements. *International Journal of Mechanical Sciences* 2019;150:484–94.
- [78] Hodgson RP, Tan M, Yeo L, Friend J. Transmitting High Power RF Acoustic Radiation via Fluid Couplants into Superstrates for Microfluidics. *Applied Physics Letters* 2009;94(2):024102.